JOURNAL OF MATERIALS SCIENCE **37** (2002) 5345 – 5353

Laser cladding of Co-based hardfacing on Cu substrate

G. DEHM*, M. BAMBERGER
Department of Materials Engineering, Technion-Israel Institute of Technology, Haifa 32000, Israel
E-mail: mbamber@mit.edu

Cu substrates were subjected to laser cladding with Triballoy 66 SNF by means of a CW-CO_2 laser, preceded by the deposition of an intermediate layer containing Cu-Ni-B-Si for improving the energy coupling between the laser radiation and the substrate. The intermediate layer is copper-rich close to the substrate and poor in copper at a distance from it. In the clad itself there is no copper. The matrix of the coating is βCo, because alloying with Mo, Cr, and Si, in combination with rapid cooling, prevented its transformation to α-Co. Part of the structure is equiaxial because of undercooling, the balance is dendritic, which is typical of laser cladding

1. Introduction

High-power CO_2 lasers find applications in many types of metal processing, such as cutting, welding, and surface treatments [1–3]. The latter group includes surface cladding, which is a technique to provide a metal substrate with a wear or corrosion-resistant layer [4]. Laser surface cladding enables the production of surface layers having properties that cannot be achieved by other means and at the same time are signalized by excellent bonding to the substrate and by minimal effect on the bulk properties of the substrate. The high rate of cooling leads to grain refinement and often results in microstructures that are not in thermodynamic equilibrium [5]. Such layers may exhibit better properties than those produced by other deposit-welding techniques.

Volz [6] reports on the cladding of copper moulds with NiCrBSi using high power CO_2-lasers. To reduce reflection of the laser beam he coated the surface prior to laser cladding, with the clad material using the thermal spraying technique. No details of microstructures, adhesion to the substrate, and, other properties of the layers are given. Laser cladding of aluminum alloys with nickel alloys has been reported by Ferraro *et al*. [7] and by Volz [6]. Ferraro [7] did not succeed in producing layers without cracks, pores, and a massive uptake of aluminum, whereas Volz [6] reports on the successful cladding of valve seats. However, his micrographs show significant zone of dilution between the layer and the substrate. This deficiency severely limits the applications of these materials, as they do not posses sufficiently good surface properties for aggravated wear and corrosion conditions such as elevated temperatures, and abrasion.

A recent report [8] deals with a cladding of a Ni-based alloy on Cu substrates with a good adhesion between the clad and the substrate, using a thin precoating to improve the absorption of the laser radiation by the substrate. Very limited dilution of the cladding with elements of either the precoating or the substrate was found, hence an improvement in the wear properties was achieved. On the other hand, other coating techniques (e.g. plasma spraying, electrodeposition) often

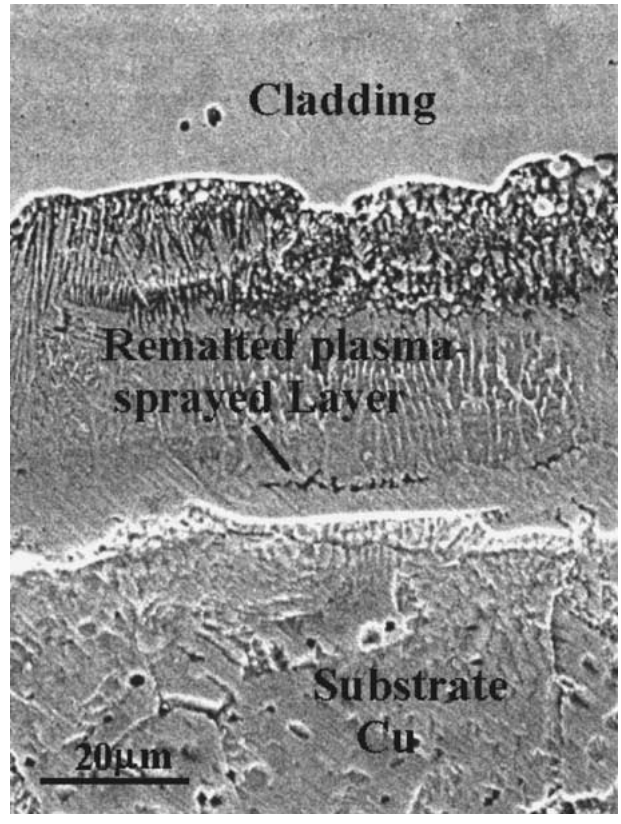

Figure 1 The SEM image shows the remelted plasma-sprayed layer between the cladding and the substrate.

Present Address: Max Plank Institut fuer Metallforschung, Stuttgart, Germany.

fail due to the poor adhesion of the coatings to the substrate. In the present study hard-facing made of Triballoy 66FNS was cladded on a Cu substrate, with the additional aim of minimizing its dilution with Cu while maintaining a strong bond to the substrate. Potential applications can be found as chill dies for continuous casting and commutators in electric motors or switching gears.

2. Experimental

Prior to cladding, copper substrates (99.9% Cu) were sandblasted and then pre-coated by plasma-spraying a layer consisting of Ni, B and Si in order to improve the absorption of the laser energy. The composition of the precoating was 95at.%Ni, 2.5at.%B, and 2.5at.%Si. This layer was subsequently laser-remelted with a cross-flow CO_2 laser (Heraeus C76) having a rectangular beam profile (size: $15 \times 25\,mm^2$). The Triballoy 66FNS (Co-28%WtMo-8%WtCr-2%WtSi, particle size $-45 + 15\,\mu m$) was cladded under the following conditions : laser power -3.6 kW, scan speed -200 mm/min, 40% overlap between successive laser tracks.

The microstructure and phase evolution of the Co-based claddings were determined by X-ray diffraction (XRD), optical microscopy, scanning electron microscopy (SEM), and transmission electron microscopy

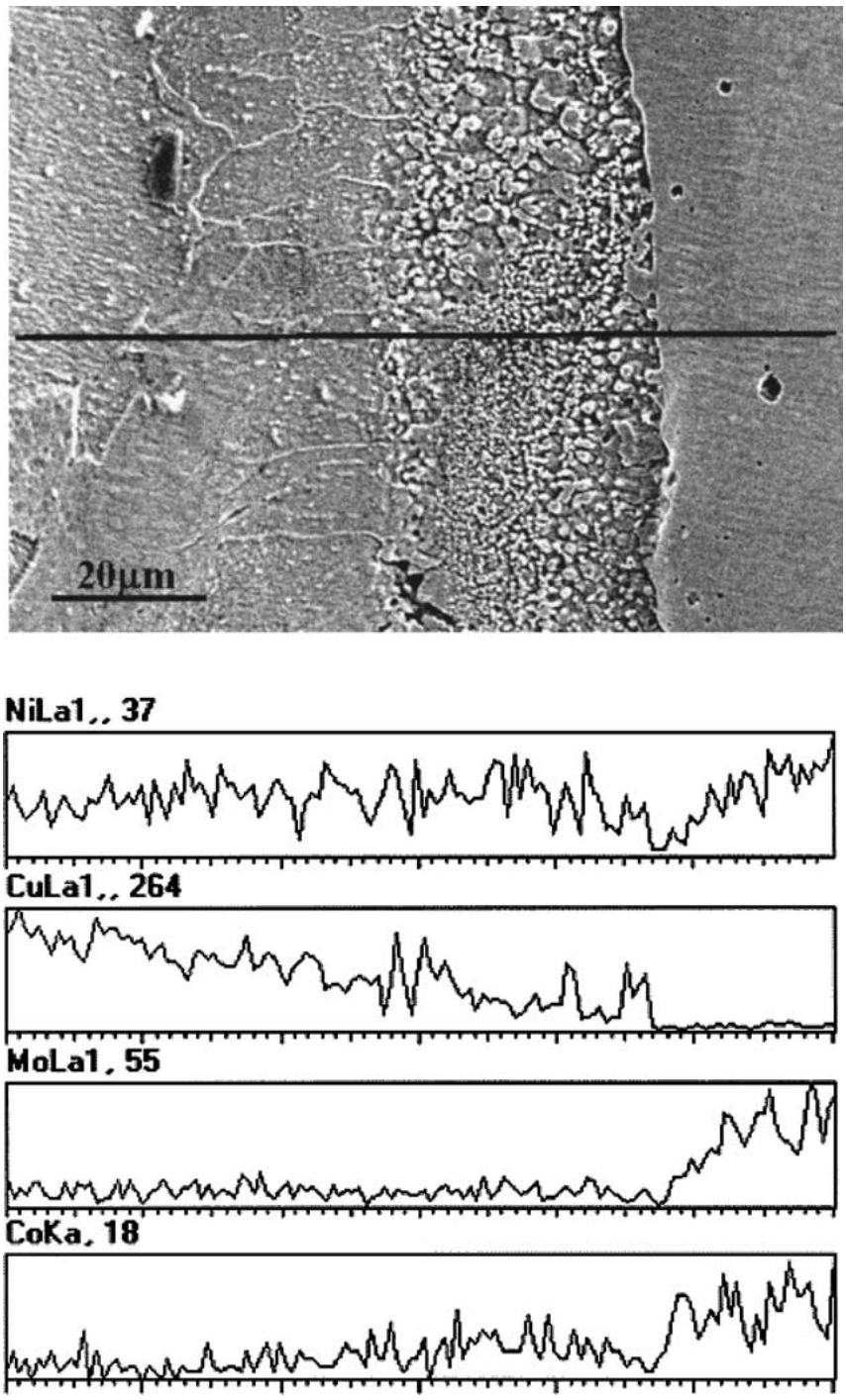

Figure 2 SEM micrograph of the cladding/remelted plasma-sprayed layers/substrate region and corresponding Co, Mo, Ni and Cu EDS line-scans (acquired along the indicated line, in arbitrary units).

(TEM). The XRD, optical microscopy and SEM examinations were made on polished and polished and etched samples. XRD measurements were performed on plan view samples in a conventional automatic powder X-ray diffractometer (Philips, PW-1820 goniometer) with a Cu Kα tube operated at 40 mA and 40 kV. 2θ-scans were obtained in the range, 20° to 90°, with a step size of 0.02° and exposure time of $\geq$2 s per step. Microstructural features of the laser-clad layers were obtained using a JEOL JSM-840 SEM, equipped with an energy-dispersive X-ray spectrometer (EDS). EDS measurements provided information on the phase composition. The EDS detector (Link 6506) possesses an atmosphere thin window for the detection of light elements ($Z > 4$). A detailed study of the laser-clad specimens microstructure was carried out with a conventional TEM using selected area diffraction (SAD). The chemical composition of the phases was determined by analytical TEM. Conventional and analytical TEMs were performed with a JEOL 2000FX (200 kV) equipped with an EDS detector (Link AN10000) capable of detecting elements

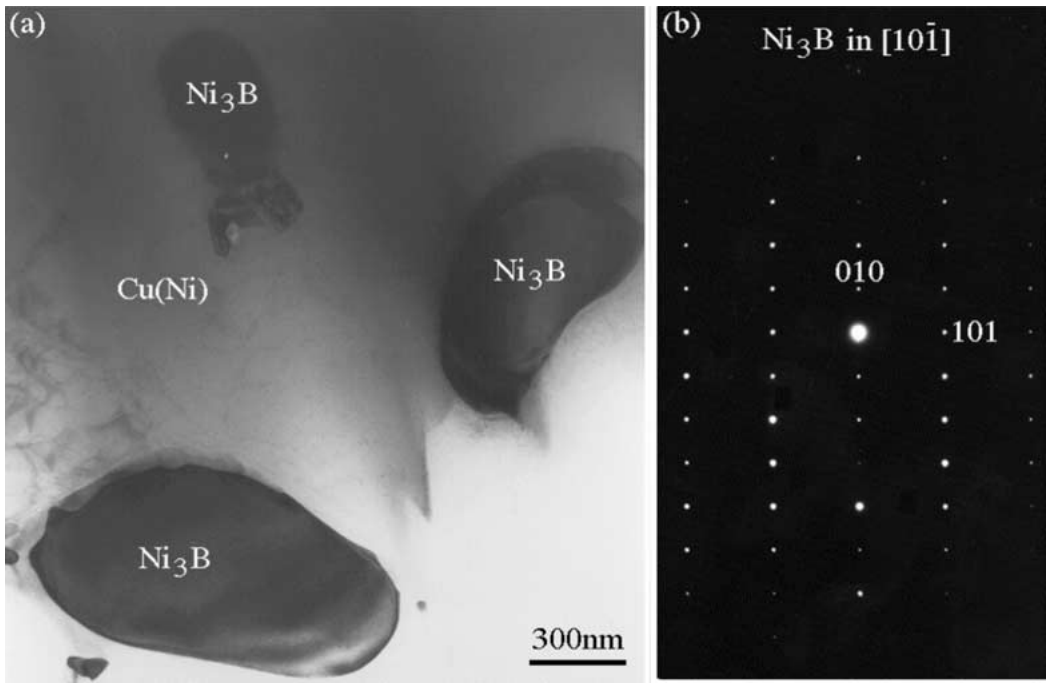

Figure 3 (a) Cu grains, which are several μm large, form the matrix of the remelted plasma-sprayed layer. The Cu grains contain Ni_3B inclusions, as detected by (b) SAD.

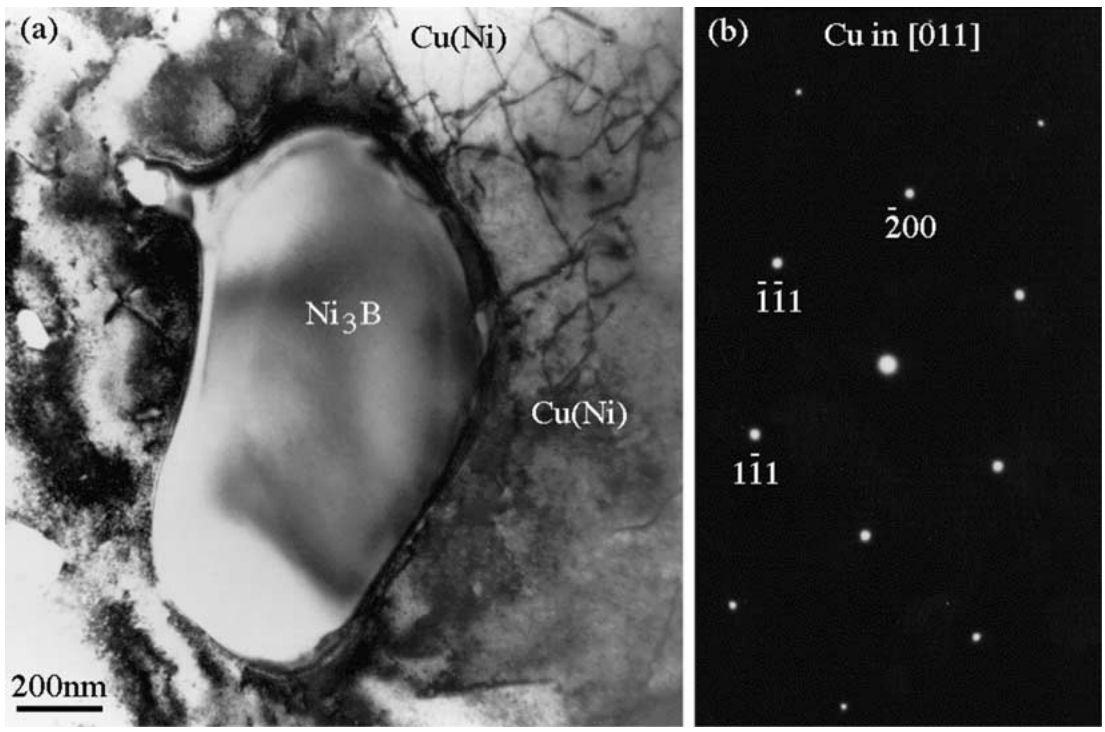

Figure 4 (a) Bright-field TEM micrograph of a Cu(Ni) grain containing a Ni_3B grain. (b) Corresponding SAD pattern of Cu along [011] zone axis.

with $Z > 10$. For the TEM studies cross-sectional and plan view foils were prepared.

3. Results

The cross-sectional SEM image presented in Fig. 1 reveals three main regions of the sample: cladding layer, plasma sprayed layer (the interlayer), and substrate.

The results show that the overall thickness of the coatings is in the range, 1–1.36 mm, depending on the thickness of the pre-coating. Using a thin pre-coating (20–30 μm) results in a thin clad; increasing the pre-coating to 30–40 μm leads to a thicker clad track. The SEM image also shows that the Cu substrate has recrystallized in the vicinity of the plasma-sprayed layer due to the laser irradiation during the cladding process. The recrystallized heat-affected zone (HAZ) extends to a thickness of 20–25 μm. Fig. 2 presents a SEM image of the cladding/interlayer/substrate region and the corresponding Cu, Ni, Co, and Mo EDS line-scans (obtained along the line indicated in Fig. 2). The line-scans reveal that the chemical composition changes abruptly at the cladding/interlayer interface, whereas at the matrix/interlayer interface a monotonic decrease of the Cu content towards the cladding is observed.

Analytical SEM examination shows that the overall chemical compositions of the cladding and of the remelted plasma-sprayed layer coincide with those of the initial powders. This means that none of the components evaporated to a detectable degree during the laser treatment.

A quantitative SEM analysis of the microstructure and the chemical composition of a cross-section of the samples reveals a significant change in the chemical composition at the matrix/interlayer interface. In the

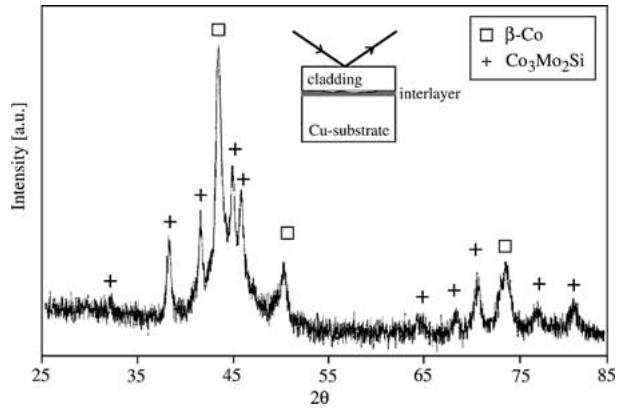

Figure 6 XRD pattern obtained at the Triballoy cladding surface and indicating the formation of βCo and Co_3Mo_2Si.

interlayer itself and close to the cladding, concentration of up to 7.3wt%Co, up to 23.7wt%Ni, up to 7wt%Cu, up to 2wt%B, up to 1.8wt%Cr, and up to 2wt%Mo were detected by EDS. Close to the substrate, on the other hand, only minor contents (less then 2wt%) of Co, Mo, and Cr, but large amounts of Cu (66wt%) and Ni (19wt%) were detected by EDS.

Cross-sectional TEM of the remelted plasma-sprayed interlayer between the substrate and the cladding reveals Cu and Ni_3B grains (Figs 3 and 4). The Cu grains, which are several μm large, constitute the matrix of the remelted plasma-sprayed layer. All analyzed Cu grains (about 20) contained Ni in solid solution as determined by EDS, indicating that remelting the plasma-sprayed layer caused (some) intermixing of the substrate with it. The Ni_3B grains, which are typically smaller than 2 μm, also contain Cu in solid solution. The EDS results are summarized in Table I. No

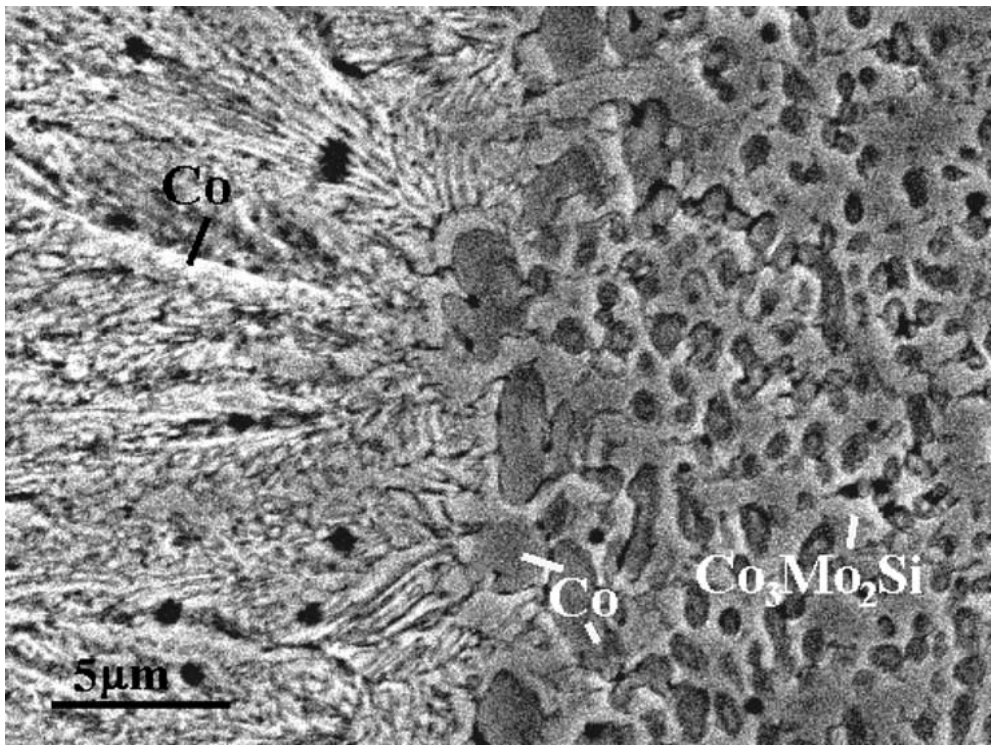

Figure 5 The SEM image shows the microstructure of the cladding (zone of the Co, Co_3Mo_2Si grains).

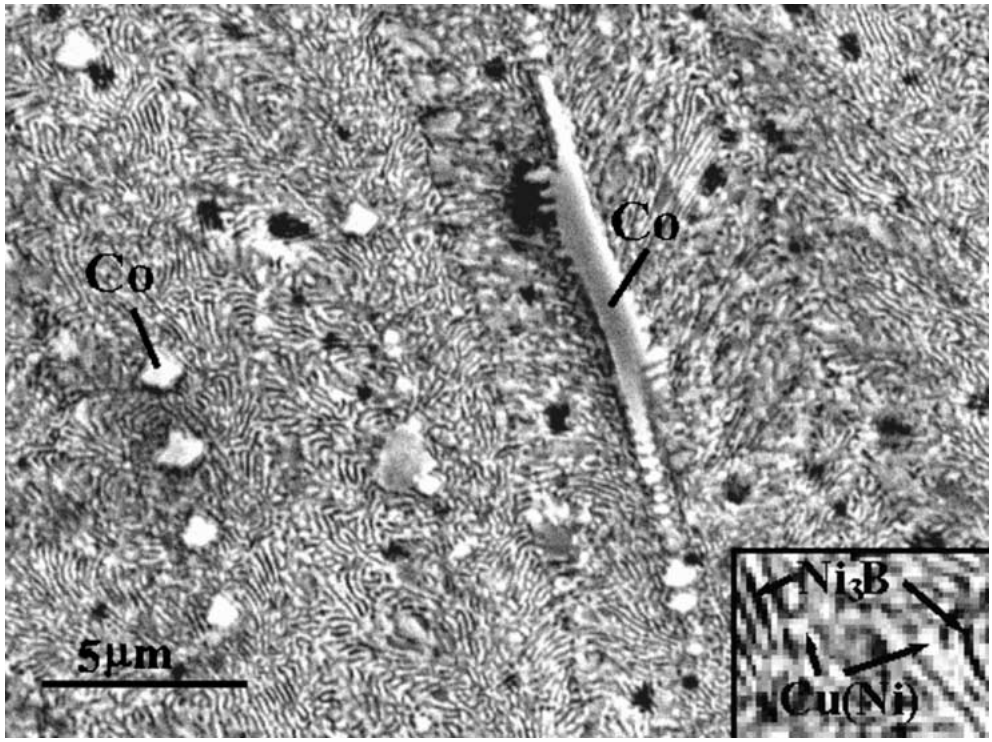

Figure 7 The SEM image shows the microstructure of the cladding close to the interlayer (zone of Co, Cu(Ni), Ni_3B grains).

TABLE I Chemical compositions of Co and Co_3Mo_2Si grains located in the cladding and of Cu(Ni) and Ni_3B grains contained in the plasma-sprayed layer, as determined by EDS in the TEM

Phase	Co	Mo	Cr	Si	Cu	Ni
β-Co	68–75	12–19	11–12	1–2	–	–
Co_3Mo_2Si	51–58	26–30	8–9	6–8	–	–
Cu(Ni)	<1	<1	<1	<1	∼74	∼22
Ni_3B*	<3	<1	<1.8	<1	∼8	∼63

Co or Co_3Mo_2Si grains were detected in the interlayer, which indicates a limited intermixing of the cladding and the plasma-sprayed layer. Cr, Co, and Mo impurities were found to be less than (1–3)at.% in the Cu(Ni) and Ni_3B grains.

The microstructure of the *cladding* is presented in Fig. 5. Close to the surface of the specimen, grains of 1–3.5 μm in diameter. are embedded in a second phase. EDS measurements show that these grains consist mainly of Co, while the second phase contains large amounts of Co, Mo and Si (53.8at.%Co, 28.8at.%Mo, 7.6at.%Si) and is most likely Co_3Mo_2Si, as suggested by the XRD analysis (Fig. 6). However, the large number of reflections present in the XRD pattern strongly suggest that other phases, such as $Cr_{0.549}Co_{1.539}Mo_{0.912}$, $Cr_{0.46}Co_{0.4}Si_{0.14}$, CrCo, or Co_2Mo_3 can also be formed in the cladding. The dendrites seen in Fig. 5 contain mostly Co and, based on the XRD pattern, are fcc - β-Co.

The microstructure of the cladding closer to the interlayer also contains, in addition to β-Co and Co_3Mo_2Si, Cu(Ni) and grains of Ni_3B (Fig. 7), which are revealed in the XRD pattern (Fig. 8); but the exact location of the last-named phase could not be determined by XRD, whether in the clad or in the interlayer.

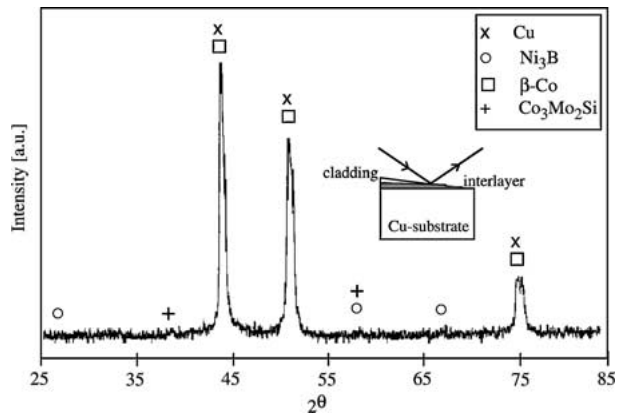

Figure 8 XRD pattern taken in the region cladding/plasma-sprayed layer/substrate interface resolving reflections of β-Co, Co_3Mo_2Si, Ni_3B, and Cu.

A detailed study of the Triballoy-clad specimens was carried out using SAD and EDS* analysis in the TEM. Plan-view TEM samples to study the phases of the cladding, and cross-sectional TEM foils were used to investigate the remelted plasma-sprayed layer between the substrate and the cladding.

The bright-field TEM pictures of the cladding reveal β-Co grains, which are several μm large (Figs 9 and 10). SAD performed on the Co grains are in agreement with the XRD results and demonstrate that Co has solidified as β-Co in the fcc structure (Fig. 9b). In the Co grains inclusions of a second phase appear (Fig. 9) and were identified by SAD (Fig. 9c) as the hexagonal Co_3Mo_2Si phase. No orientational relationship exists between the

* The EDS system of the TEM is not capable of detecting B. Thus, a fixed concentration of 25at.% B was assumed for the EDS analyses of Ni_3B grains.

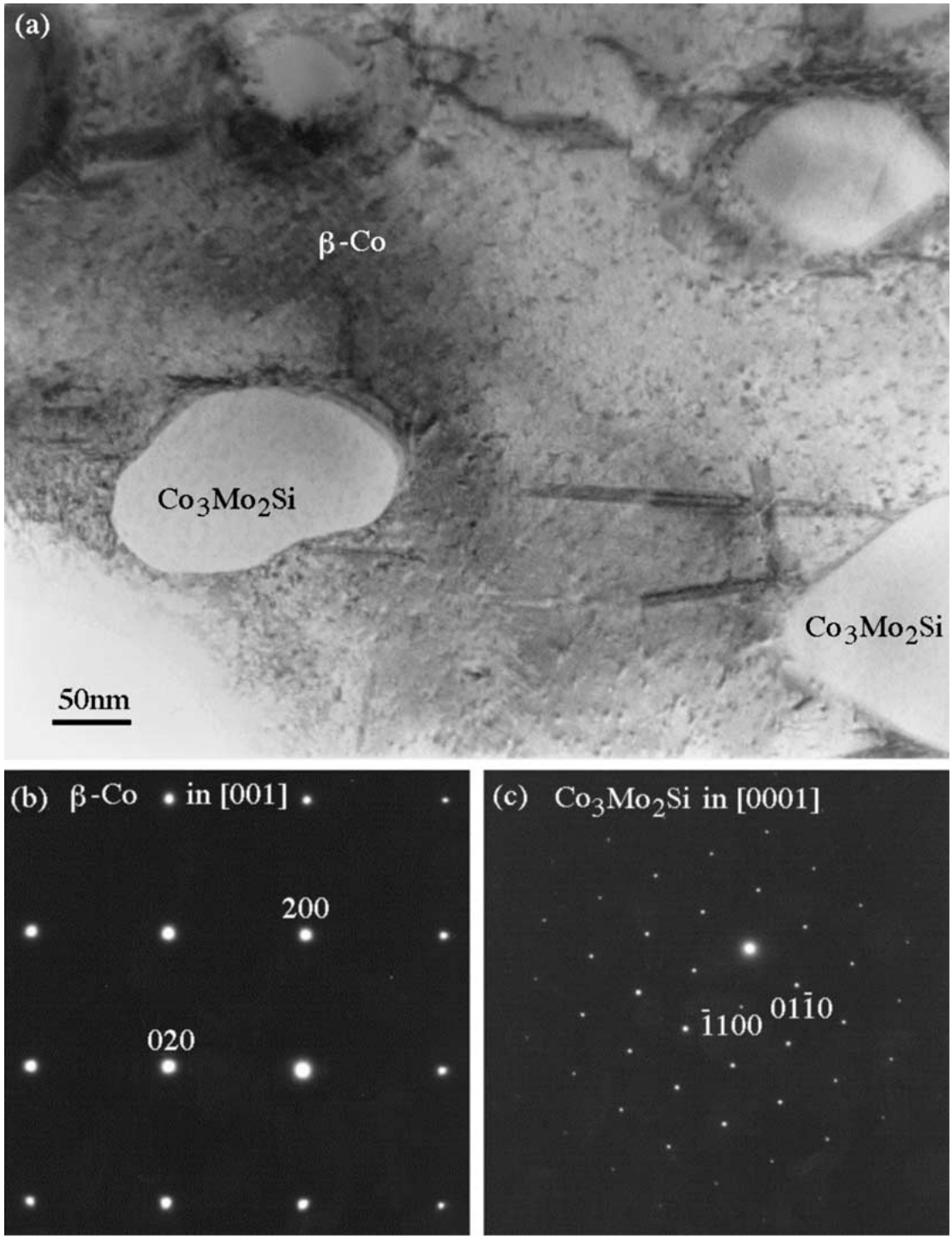

Figure 9 (a) Bright-field TEM image of a β-Co grain containing Co_3Mo_2Si inclusions. SAD patterns of (b) β-Co along the [001] zone axis and (c) of Co_3Mo_2Si along the [0001] zone axis.

two phases, thus each grain has to be tilted into a low-indexed zone axis in order that SAD patterns can be obtained. Fig. 9a and b show the SAD patterns of β-Co along the [001] zone axis and of Co_3Mo_2Si along the [0001] zone axis.

Co tends to grow as dendrites, as can be seen in the bright-field TEM micrograph of Fig. 10. The β-Co dendrite arms are engulfed by grains of Co_3Mo_2Si. The polycrystalline Co_3Mo_2Si grains are typically 100–300 nm in size and solidify along the dendrite arms. However, a few large equiaxed β-Co grains are also present in the cladding. These Co grains contain a number of Co_3Mo_2Si inclusions (Fig. 11). No further phases in the cladding were observed by TEM. Thus the XRD and TEM results indicate that the Triballoy cladding consists solely of β-Co and Co_3Mo_2Si.

The β-Co grains frequently exhibit a large number of faults when they are tilted parallel to a [011] zone axis (Fig. 12). These faults run along (111) Co planes and cause streaks in the diffraction pattern along the [111] directions (Fig. 12b and c). The faults are assumed to be stacking faults on (111) planes. EDS analyses of the Co grains show that they consist of (68–75)at.%Co, (12–19)at.%Mo, (11–12)at.%Cr, and (1–2)at.%Si (Table I).

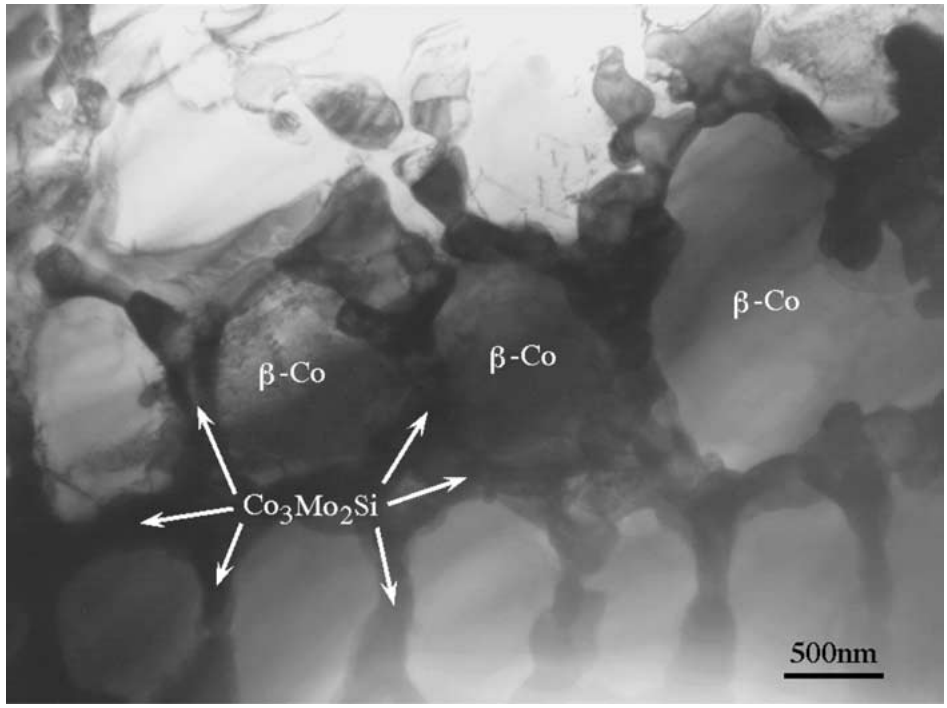

Figure 10 The bright-field TEM micrograph shows β-Co dendrite arms which are engulfed by Co_3Mo_2Si grains. The polycrystalline Co_3Mo_2Si grains are typically 100–300 nm in size.

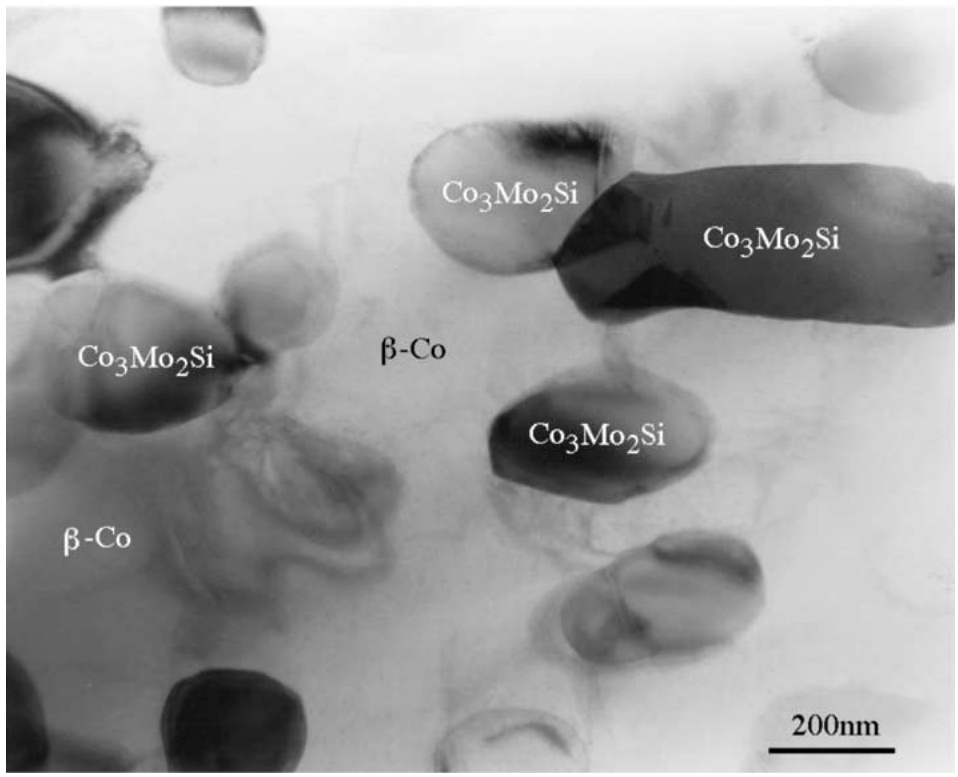

Figure 11 Equiaxed β-Co grains contain a number of Co_3Mo_2Si inclusions.

Both effects, rapid cooling and alloying elements, are known to prevent the β-Co $\rightarrow$ α-Co transformation.

Analytical TEM was also applied on the Co_3Mo_2Si grains. The EDS results yield a chemical composition of (51–58)at.%Co, (26–30)at.%Mo, (8–9)at.%Cr, and (6–8)at.%Si (Table I). The Cr content of (8–9)at.% is probably due to partial replacement of Si with Cr, the total amount of Cr and Si being (15–16)at.% in the Co_3Mo_2Si phase.

4. Discussion

The coefficient of reflection of CO_2 laser radiation from copper is very high [9], and in addition copper has a high thermal conductivity. In order to melt the surface of a copper substrate, therefore, either a very-high-power CO_2 laser (8–10 kW) must be employed or the energy coupling must be improved by a suitable coating as was done in the present case. Plasma-coating with a layer of Ni-Si-B on a Cu substrate enabled the melting of both

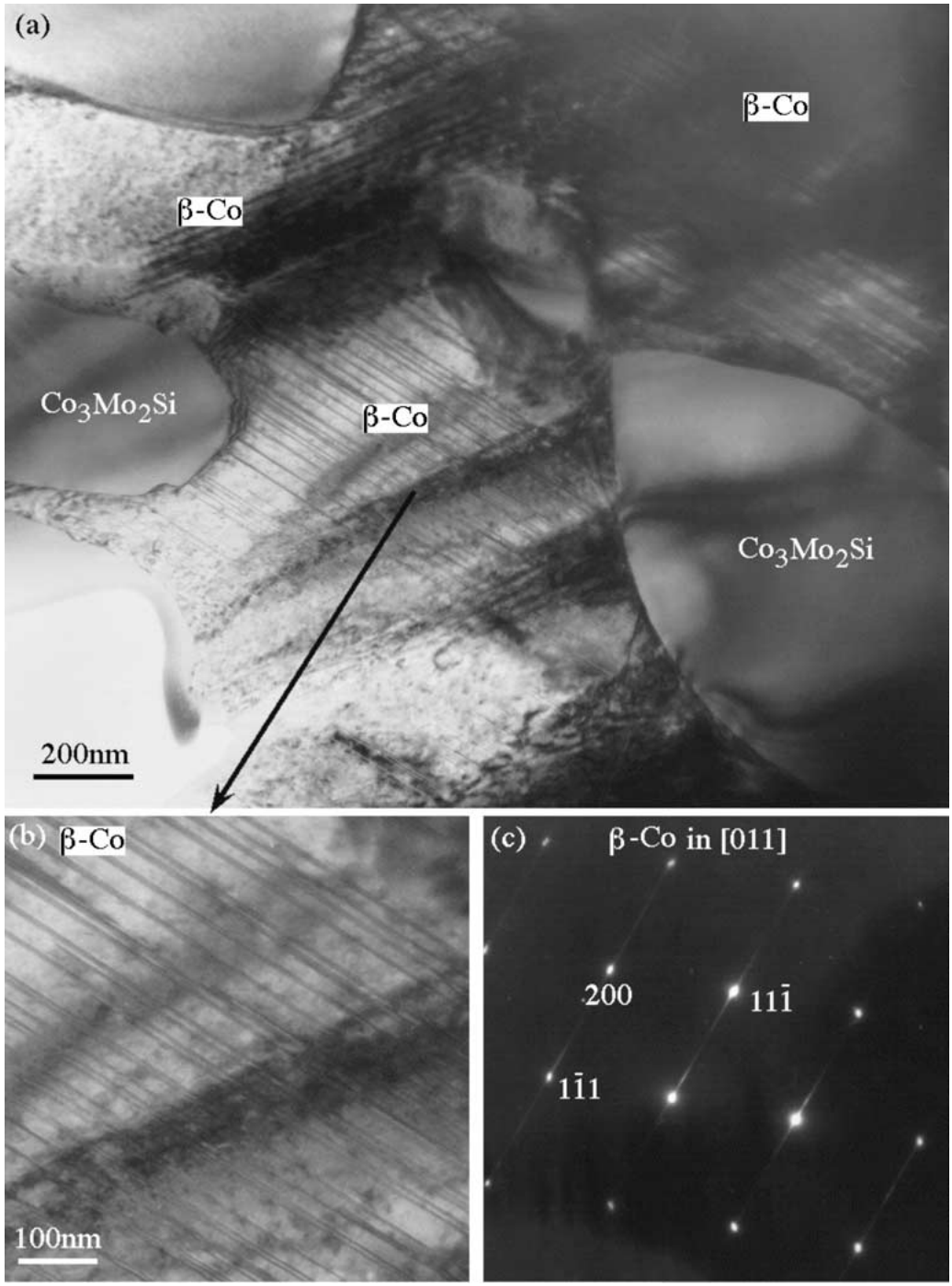

Figure 12 (a) Bright-field TEM micrograph of a β-Co grain with (b) faults on (111) Co planes as determined (c) by SAD. The faults indicate incomplete transformation from the fcc β-Co to the hcp α-Co structure.

the coating material and the surface of the substrate with a CW-CO_2 laser of only 3.6 kW output. The surface obtained after the first melting had a thermal conductance lower than that of copper, it was rough and did not reflect the radiation as perfectly as does virgin copper. It was thus possible to melt the Triballoy powder together with the copper surface and to produce a clad on the copper substrate. Melting the coating layer was accompanied by a melting of the substrate surface, which caused a very high concentration of Cu in the interlayer close to the surface, as determined by compositional analysis and x-ray diffraction. The rapid solidification of a relatively thin liquid layer (less than 100 μm) on a substrate of excellent heat conductance apparently led to very high overcooling and to homogeneous nucleation in the interlayer rather than to dendritic growth (Fig. 3). On the other hand, in areas in which complete bond with the substrate did not occur, which is manifested, for example, by the crack seen in Fig. 1, the rate of cooling was lower, and this made the dendritic growth possible (Fig. 1).

The renewed irradiation of the surface during the actual cladding caused the complete melting of the Triballoy powder and the formation of a coating 1 mm thick, but only a partial melting of the interlayer. This is why the interlayer close to the clad contains over 70% Co and little Cu, whereas in the vicinity of the substrate there is no Co but 66% Cu. The decrease of the copper

content in the interlayer is clearly seen in the line scan (Fig. 3). If the interlayer had been completely melted, a more homogeneous composition would have resulted owing to the turbulent flow characteristic of surface melting by laser. Furthermore, the fact that the composition of the clad is very near to that of the original powder proves once again that no melting to any depth occurred in the interlayer, so that dilution of the clad with elements from the substrate or from the precoating was prevented. Adjacent to the interlayer, elements were found in the clad that stemmed from the interlayer—B, Cu—which once again proves the melting of the substrate surface during the cladding to have been limited. A thick layer of melt prevented the very rapid solidification to an equiaxial structure but led to dendritic growth from the substrate towards the surface. The latter, for its part, being exposed to the environment apparently either underwent more rapid cooling, or the local changes in its composition during solidification in combination with undercooling led to eutectic solidification even though the composition of the melt deviated from the eutectic [10]. The structure near the surface, therefore, differs from the dendritic structure of the clad layer as a whole (Fig. 5). In any case the phase that solidifies first is Co, and thus the residual melt is enriched by the alloying elements Mo and Si, creating the intermetallic compound, Co_3Mo_2Si, among the Co grains. At a certain distance from the surface dendritic Co is obtained, and between its arms Co_3Mo_2Si is dispersed. In the cladding close to the interlayer Cu(Ni) and Ni_3B are found. These phases are caused by the partial melting of the interlayer and the segregation of Ni, Cu, and Si into the residual melt between the dendritic arms of Co.

Analyses of the composition of the Co grains in the outer portion of the clad and of the Co dendrites in any part of it showed that Co dissolves Mo to the extent of 12–19%, Cr to 11–12%; and Si between 1–2%. That alloying of the Co together with the rapid cooling slow down the transformation from fcc β-Co, which is stable at high temperatures, to hcp-α-Co, which is stable only at lower temperatures. The fact that the transformation from fcc-β-Co to hcp-α-Co was not complete finds expression in the faults detected in the fcc-β-Co.

Analytical TEM was also applied on the Co_3Mo_2Si grains. The EDS results yield a chemical composition of (51–58)at.%Co, (26–30)at.%Mo, (8–9)at.%Cr, and (6–8)at.%Si (Table I). The Cr content of (8–9)at.% is probably due to replacement of Si by Cr, the total amount of Cr and Si being (15–16)at.% in the Co_3Mo_2Si phase. On the other hand the heating caused by the successive passage of the laser leads to the precipitation of fine-grained Co_3Mo_2Si within the β-Co without any orientational relationship between the two.

5. Conclusion

- Triballoy cladding of copper substrates is possible with a CW-CO_2 laser having a 3.6 kW output following prior coating with such alloys as NiCrSi in order to improve the energy coupling between the laser and the substrate.
- The nature of the solidification in the interlayer between the substrate and the cladding depends on the heat transfer to the substrate: If the thermal contact is good, cooling of the molten surface layer is very rapid, homogeneous nucleation and a spherolitic structure in the layer result. In other areas, in which a crack is discovered between the substrate and the interlayer, the rate of cooling is not so high, and dendritic growth is the result. The rate of cooling similarly affects the nature of the solidification of the cladding.
- The composition of the melt depends on its distance to the interlayer—close to the interlayer it is enriched with Cu and B but at a distance Mo, Cr and Si dominate. Therefore, in the course of the solidification of the primary fcc- β-Co, the elements Cu and B precipitate in a zone adjacent to the interlayer, whereas in a zone at a distance from the interlayer Mo, Cr and Si precipitate. This is evident from the formation of Ni_3B and Cu(Ni) between the Co dendrites arms close to the interlayer and of Co_3Mo_2Si elsewhere.
- The rapid cooling and the dissolution of Cr, Mo, Si, in the fcc β-Co prevent the transformation, β-Co $\rightarrow \alpha$-Co, whereas heating the supersaturated Co causes the precipitation of fine-grained Co_3Mo_2Si within it.

Acknowledgement

The study was partially supported by the fund of the Vice-President of Technion for Research. Dr G. Dehm acknowledges the Alexander von Humboldt society for supporting his study at the Technion. Prof. B. L. Mordike and Dr. S. Mordike, Institut fr Werkstofftechnik und Werkstoffwissenshaft der TU Clausthal,Germany, are acknowledged for the laser cladding and Dr. L. Shepeleva, Department of Materials Engineering Technion, for the SEM analysis.

References

1. B. L. MORDIKE, *J. De Physique Colloque C7* **48** (Supp.12) (10 87) C7-37.
2. M. BOAS and M. BAMBERGER, *Wear* **126** (1988) 219.
3. A. OHMORI and K. KAMADA, *Trans. JWRI* **18**(2) (1989) 143.
4. B. L. MORDIKE, in Proc. Conf. ECLAT 90, Sept. 17–19, 1990, Erlangen Germany, p. 371.
5. M. FASTOW, M. BAMBERGER, N. NIR and M. LANDKOFF, *Materials Science and Technology* **6** (1990) 900.
6. R. VOLZ, in Proc. Conf. ICALEO 93, Oct. 24–28, 1993, Orlando, FL, USA, LIA 77, p. 999.
7. F. FERRARO, C. A. NANNETTI, M. CAMPELLO and A. SENIN, in Proc. Conf. Lasers in Manufacturing June 3–5, 1986, Paris, France, p. 233.
8. G. DEHM, B. MEDRES, L. SHEPELEVA, C. SCHEU, M. BAMBERGER, B. L. MORDIKE, S. MORDIKE, G. RYK, G. HALPERIN and I. ETSION, *Wear* **225–229** (1999) 18.
9. W. M. STEEN, "Laser Material Processing" (Springer-Verlag, Berlin, 1991) p. 266.
10. W. KURZ and D. J. FISHER, "Fundamentals of Solidification" (Trans Tech Publications, Switzerland, 1984) p. 27.

Received 2 February
and accepted 16 July 2001